European Journal of Chemistry

View Journal Online
View Article Online

Synthesis, crystal structure, Hirshfeld analysis and computational studies of a novel cadmium(II) complex derived from 2-benzoylpyridine-N^4-ethyl thiosemicarbazone

Alan Mankottil Johnson, Nisha Kuttappan and Kannan Vellayan *

Department of Chemistry, Government College Kattappana, Kerala-685508, India

** Corresponding author at: Department of Chemistry, Government College Kattappana, Kerala-685508, India.*
e-mail: kannanpvl@gmail.com (K. Vellayan).

RESEARCH ARTICLE

10.5155/eurjchem.17.1.79-88.2784

Received: 29 January 2026
Received in revised form: 25 February 2026
Accepted: 3 March 2026
Published online: 31 March 2026
Printed: 31 March 2026

KEYWORDS

DFT
MEP
Hirshfeld analysis
Thiosemicarbazones
Cadmium(II) complex
X-ray diffraction analysis

ABSTRACT

A novel sulfur-bridged box dimer cadmium complex, $[Cd_2(bzpyetsc)_2(Cl)_2]$, of 2-benzoylpyridine-N^4-ethyl thiosemicarbazone [Hbzpyetsc] ligand prepared and characterized by various physicochemical methods, single crystal X-ray diffraction studies and spectroscopic methods. Single crystal X-ray diffraction studies showed that the prepared complex has a distorted square pyramid coordination around cadmium(II) and the compound crystallized in the monoclinic space group $C2/c$. The intermolecular hydrogen bonding and weak interaction provide a 2-dimensional laminar structure for the complex. The infrared spectra of the complex revealed that the thiosemicarbazone ligand coordinates to the metal center in its deprotonated thiolate form through the pyridine nitrogen, azomethine nitrogen and thione sulfur atoms. The electronic spectral data showed that the bands assigned to the azomethine bond in the ligand are slightly shifted upon complexation. Furthermore, the complex was optimized and evaluated computationally using the density functional theorem. The HOMO-LUMO analysis revealed that the energy gap is 1.876 eV. Theoretical investigations of the prepared complex are performed by Frontier molecular orbital and molecular electrostatic potential analysis to understand the electron distribution. From the MEP study, it was found that the electron density is predominantly localized around chlorine atoms. Hirshfeld analysis proved that the H-H interaction is the most notable intermolecular interaction.

Cite this: *Eur. J. Chem.* **2026**, *17(1)*, 79-88 **Journal website**: www.eurjchem.com

1. Introduction

The interesting field of coordination chemistry exhibits the notable ability of metal ions to form bonds with a wide variety of ligands. The transition-metal complex synthesized using organic ligands containing N and S heteroatoms as coordination sites is particularly important. The imine derivative ligand, thiosemicarbazone, has a wide range of biological properties [1,2]. Thiosemicarbazone multidentate ligands are more flexible and are sulfur-nitrogen-containing Schiff base ligands. Their conformational flexibility and the presence of different potential donor atoms allow for various modes of coordination with metal ions. Because of their diverse range of functions and stereochemical binding modes, a wide range of transition-metal complexes using thiosemicarbazones have been synthesized in recent years.

Cadmium belongs to the *d*-block element and its electronic configuration is $4d^{10}5s^2$. The divalent (+2) oxidation state is more stable due to the closed d-shell. As a result of crystal field stabilization, the cadmium(II) ion with its d^{10} configuration displays a variety of coordination geometries based upon the interaction of electrostatic effects, the covalency, and the size factor. The main coordination numbers observed for Cd(II) are 4, 5, and 6. Because the ionic radius of cadmium(II) is significantly larger, it exhibits a high preference for the formation of six coordinated octahedral species. Cadmium ion is widely used in the field of batteries, industrial plating, and as a pigment in plastics [3]. Cadmium complexes have potential for the treatment of cancer, but due to toxic side effects, their use is often limited [4]. Cadmium prefers easily oxidizable soft ligands, as the Cd^{2+} ion is considered a soft Lewis acid, but it is not a typical soft ion. It has a high degree of polarizability and its complexes with soft ligands have predominantly covalent bond characteristics. The stability of cadmium complexes varies, depending on the types of ligands. Due to its versatile coordinating abilities, Cd(II) gives simple complexes and even 1D, 2D, and 3D polymeric structures, showing numerous applications. These polymers exhibit interesting physical properties. Cd^{2+} is capable of forming the most stable complexes with soft donor atoms (S > N > O). Typically, the stability of the complexes increases with the number of coordination groups contributed by the ligand; therefore, the complexes of Cd^{2+} with polydentate ligands containing SH groups are very stable. Cd(II) shows a strong interaction with the S^{2-} group and forms highly stable complexes [5-11].

https://dx.doi.org/10.5155/eurjchem.17.1.79-88.2784

Table 1. Crystal data and structure refinement parameters of $[Cd_2(bzpyetsc)_2(Cl)_2]$.

Parameters	$[Cd_2(bzpyetsc)_2(Cl)_2]$
Empirical formula	$C_{30}H_{30}Cd_2Cl_2N_8S_2$
Molecular weight	862.48
Color	Yellow
Temperature (T) K	296(2)
Wavelength (Mo Kα) (Å)	0.71073
Crystal system	Monoclinic
Space group	*C*2/*c*
Cell parameters	
a	20.9473(8)Å
b	12.3048(8)Å
c	16.1750(9)Å
α	90°
β	125.339(3)°
γ	90°
Volume V ($Å^3$)	3401.0(3)
Z	4
Calculated density (ρ) (mg m^{-3})	1.684
Absorption coefficient, μ(mm^{-1})	1.564
F(000)	1712
Crystal size (mm^3)	0.50 x 0.45 x 0.40
θ range for data collection	2.59 to 28.00°
Limiting indices	$-27 \le h \le 23, -16 \le k \le 16, -20 \le l \le 20$
Reflections collected	12530
Unique Reflections (R_{int})	4044 [R(int) = 0.0351]
Completeness to θ	28.00 (98.6%)
Absorption correction	Semi-empirical from equivalents
Maximum and minimum transmission	0.535 and 0.462
Refinement method	Full-matrix least-squares on F^2
Data / restraints / parameters	4100 / 1 / 204
Goodness-of-fit on F^2	1.161
Final R indices [I > 2σ (I)]	R_1 = 0.0299, wR_2 = 0.0702
R indices (all data)	R_1 = 0.0375, wR_2 = 0.0772
Largest difference peak and hole (e $Å^{-3}$)	0.916, -0.796

Cd(II) complexes have applications in catalysis, electrochemistry and have biological activities such as anticancer, antibacterial and antifungal activities [12-14]. Cd(II) exhibits a coordination number ranging from 4 to a 8 that corresponds to wide range of geometries [15].

Thiosemicarbazone-based ligands are well-known for their strong chelating properties via nitrogen and sulfur donor atoms, as well as their extensive coordination chemistry. Their metal complexes frequently show physicochemical and biological features in comparison to those of the free ligands. The 2-benzoylpyridine-*N*⁴-ethylthiosemicarbazone (Hbzpyetsc) ligand is of great relevance in this context, as it can coordinate metal ions across numerous donor sites, stabilizing multinuclear metal frameworks. In this paper, we have synthesized a Cd(II) complex $[Cd_2(bzpyetsc)_2(Cl)_2]$ of the ligand 2-benzoylpyridine-*N*⁴-ethyl thiosemicarbazone (Hbzpyetsc). Furthermore, we report the synthesis, molecular structure and computational work of $[Cd_2(bzpyetsc)_2(Cl)_2]$. Detailed theoretical and experimental investigations initiate to comprehend the electronic structure and other properties suitable for various potential applications. The computational investigations enabled the identification of reactive regions and the elucidation of intermolecular interactions within the system.

2. Experimental

2.1. Synthesis

We prepared a novel Cd(II) complex by refluxing an equal amount (0.5 mmol) of methanolic solution of cadmium chloride with the ligand 2-benzoylpyridine-*N*⁴-ethyl thiosemicarbazone (Hbzpyetsc). The prepared solution was cooled, filtered, and washed with distilled water. Following this, we employed a slow evaporation technique in dimethylformamide as a solvent to obtain yellow crystals of the complex. The product was subsequently characterized using spectroscopic and analytical techniques [16].

2.2. Molecular structure determination and refinement

The X-ray intensity data of 12530 reflections (of which 4044 are unique) were collected on a Bruker SMART APEXII CCD diffractometer, equipped with graphite monochromated MoKα (λ = 0.71073) radiation as the X-ray source. The crystal used for the data collection was of dimensions 0.5 × 0.45 × 0.40 mm^3. The dimensions of the unit cells were measured and the data collection was carried out at 296(2) K. The cell dimensions were determined by least-squares fit of angular settings of 4044 reflections in the θ range 2.59° to 28.00°. All non-hydrogen atoms were refined anisotropically by full matrix least square method while all H atoms on C were refined in an isotropic approximation guided by difference Fourier maps, with C-H bond distances 0.93-0.96 Å. Hydrogen atoms were assigned as U_{iso} = 1.2 U_{eq} (1.5 for Me). The H atom (N4-H4′) was located from difference maps and its distance is restrained to 0.88±0.01 Å. SMART and Bruker SAINT software are used for data acquisition and data integration, respectively [17]. Absorption corrections were carried out using SADABS based on Laue symmetry using equivalent reflections [18]. The structure was solved directly using SHELXS97 [19]. The SHELXL97 software was used to refine the structure using full-matrix least squares calculations [20]. Molecular and crystal structures were drawn with Diamond software version 3.2 [21]. The crystallographic data and the structure refinement parameters for the compound are given in Table 1. The selected bond lengths and bond angles of the complex are given in Table 2.

2.3. Computational studies

The title complex was optimized and evaluated using Gaussian 09W software [22]. Geometry optimization and frequency calculation were done using density functional theory (DFT) with the B3LYP exchange correlation functional. The LANL2DZ basis set was used for the Cd atoms and the 6-31G(d) basis set was used for the C, H, N, S, and Cl atoms [23].

Table 2. Selected bond lengths and bond angles of the cadmium complex.

Bond length	Experimental, Å	Theoretical, Å	Bond angles	Experimental, Å	Theoretical, Å
Cd(1)–N(1)	2.319(2)	2.320	N(1)–Cd(1)–N(2)	70.28(8)	70.30
Cd(1)–N(2)	2.343(2)	2.345	N(1)–Cd(1)–Cl(1)	98.97(6)	99.98
Cd(1)–Cl(1)	2.151(5)	2.155	N(2)–Cd(1)–Cl(1)	142.92(6)	145.92
Cd(1)–S(1)	2.6162(7)	2.616	N(1)–Cd(1)–S(1)	144.18(6)	147.18
Cd(1)–S(1)$^{\#1}$	2.6225(8)	2.630	N(2)–Cd(1)–S(1)	74.02(6)	75.01
S(1)–C(13)	1.770(3)	1.775	Cl(1)–Cd(1)–S(1)	107.86(3)	110.86
S(1)–Cd(1)$^{\#1}$	2.6225(8)	2.620	N(1)–Cd(1)–S(1)$^{\#1}$	98.30(7)	100.32
N(2)–N(3)	1.369(3)	1.368	N(2)–Cd(1)–S(1)$^{\#1}$	107.96(6)	107.98
N(3)–C(13)	1.308(3)	1.301	Cl(1)–Cd(1)–S(1)$^{\#1}$	108.69(3)	105.69
			S(1)–Cd(1)–S(1)$^{\#1}$	95.16(2)	95.22
			C(13)–S(1)–Cd(1)	97.53(9)	96.53
			C(13)–S(1)–Cd(1)$^{\#1}$	96.39(9)	96.55
			Cd(1)–S(1)–Cd(1)$^{\#1}$	84.05(2)	85.05

Symmetry code: #1-*x*+1, *y*, -*z*+1/2.

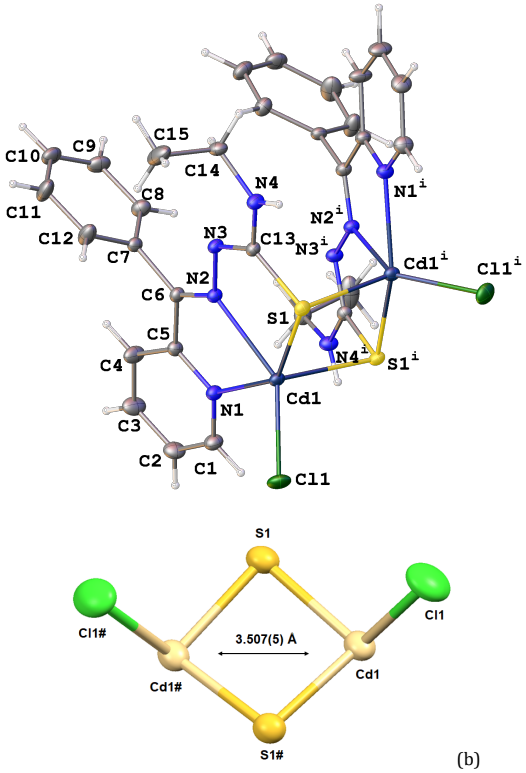

Figure 1. Molecular structure of $[Cd_2(bzpyetsc)_2(Cl)_2]$. Symmetry transformations used to generate equivalent atoms: #1 -*x*+1, *y*, -*z*+1/2.

The optimized geometry was later used to find the Frontier molecular orbital analysis (HOMO-LUMO) [24,25]. A smaller HOMO-LUMO energy gap generally indicates a higher reactivity and a lower kinetic stability. Molecular hardness is also correlated with the HOMO-LUMO gap. These analyses are very helpful for gathering information about the electronic distribution and stability of the complex. The molecular electrostatic potential (MEP) map provides information on the three-dimensional electron distribution in a molecule [26]. It specifies the regions of high and low electron density. The calculated values of the molecular electrostatic potential are usually represented with contours of the same potential in a selected plane. The title complex was color coded using the MEP diagram and the reactive and nonreactive regions was identified [27].

3. Results and discussion

3.1. Synthesis

The ligand Hbzpyetsc was prepared by the condensation reaction of 2-benzoylpyridine (0.183 g, 1 mmol) and *N*^{4}-ethylthiosemicarbazide (0.119 g, 1 mmol) in acidic condition. The ligand Hbzpyetsc (0.142 g, 0.5 mmol) and the metal salt $CdCl_2 \cdot 2H_2O$ (0.114 g, 0.5 mmol) are taken in a 1:1 molar ratio in methanol and refluxed for 4 h, resulting in the formation of $[Cd_2(bzpyetsc)_2(Cl)_2]$. The obtained crystal is separated and recrystallized.

3.2. Crystal structure analysis

The title complex was characterized using single-crystal X-ray analysis. The product crystallized in a monoclinic space group *C*2/*c* and has a distorted square pyramidal geometry. The two cadmium centers are bridged by S atoms and form a box-dimer structure. The two cadmium atoms are separated by 3.507 Å and the bridging sulfur atoms by 3.867 Å [28]. The tridentate ligand coordinates with the metal center by the formation of two fused five-membered chelate rings Cd–N–N–C–S and Cd–N–C–C–N. Each Cd(II) ion is pentacoordinated with two imine nitrogen atoms, a sulfur atom from a thiosemicarbazonate ligand, a sulfur atom of adjacent ligand acting as a bridge, and with chlorine atom. The molecular structure of the complex is shown in Figure 1.

Table 3. Interaction parameters for $[Cd_2(bzpyetsc)_2(Cl)_2]$ *.

H-bonding				
D–H···A	**D–H (Å)**	**H···A (Å)**	**D···A (Å)**	**D–H···A (°)**
N(4)-H(4')···Cl(1)#2	0.879(10)	2.513(17)	3.324(3)	154(3)
C–H···π interactions				
C-H(I)···Cg(J)	**C-H (Å)**	**H···Cg (Å)**	**C···Cg (Å)**	**∠C-H···Cg (°)**
C15-H15C···Cg(3)		2.86	3.440(7)	120
Metal···π interaction				
Cg(I)···Me(J)	**Cg···Me (Å)**	**β (°)**		
Cg(2)–Cd(1)	3.155	35.29		

* Equivalent position codes: #2=*x*, -*y*+1, *z*+1/2; Cg(2): Cd(1)–S(1)–C(13)–N(3)–N(2); Cg3: Cd(1)–N(1)–C(5)–C(6)–N(2); D = Donor, A = acceptor, Cg = Centroid of the ring; β = Angle between Cg(I)···Cg(J) vector and Cg(J) perp.

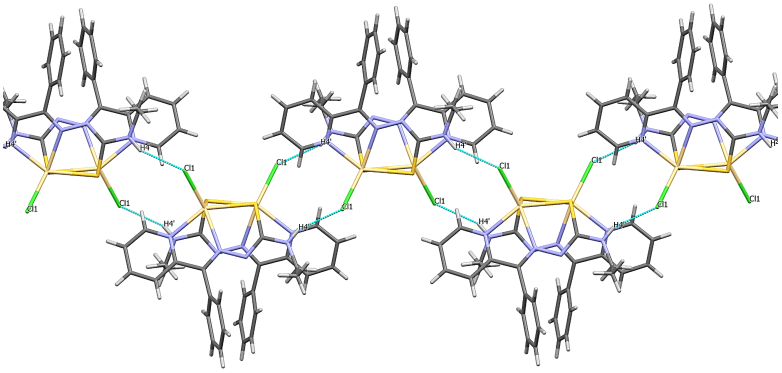

Figure 2. Intermolecular hydrogen bonding interactions for $[Cd_2(bzpyetsc)_2(Cl)_2]$.

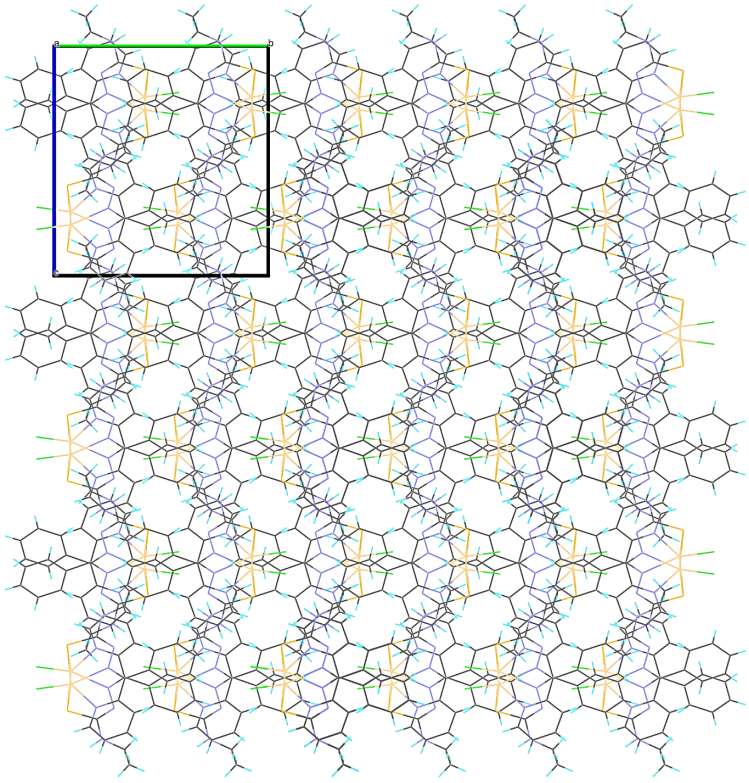

Figure 3. Packing diagram of viewed along *a* axis for $[Cd_2(bzpyetsc)_2(Cl)_2]$.

Due to the deprotonation of the ligand, the C-S bond showed larger bond distances (1.770 Å) than the normal thione bond (1.6 Å), which is between a single and a double bond, as it has been already observed in the cases of other similar species and this can confirm the deprotonation of the ligand [29]. An intermolecular hydrogen bond formed between the thioamide proton and the chloride atom. The intermolecular hydrogen bonding interactions are shown in Figure 2. Two dimer units packed in a laminar structure, resulting in a 2D network. The packing diagram of the complex viewed along *a* axis is shown in Figure 3. Several other intermolecular interactions such as weak C–H···π and metal···π bonding reinforces the crystal packing. C–H···π and metal···π interactions are shown in Figure 4. The various interaction parameters are shown in Table 3.

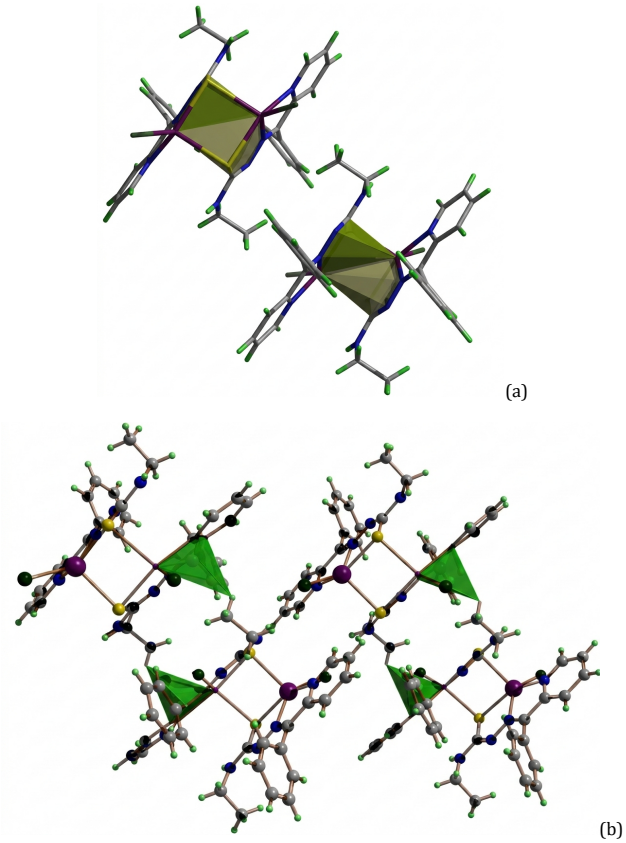

Figure 4. (a) Metal···π interaction and (b) C–H···π interactions for $[Cd_2(bzpyetsc)_2(Cl)_2]$.

The structure of the complex is further studied by elemental analysis and infrared and ultraviolet spectroscopy. IR spectral data of the free ligand (Hbzpyetsc) and its cadmium complex $[Cd_2(bzpyetsc)_2Cl_2]$ are summarized as follows: For Hbzpyetsc, the ν(C=N) stretching vibration appears at 1583 cm^{-1}, while the ν(N–N) vibration is observed at 1107 cm^{-1}. The ν(C=S)/ν(C–S) bands are detected at 1306 and 812 cm^{-1}. No ν(O–H), δ(C=S)/δ(C–S), or ν(C–O) bands were reported. For the $[Cd_2(bzpyetsc)_2Cl_2]$ complex, the ν(C=N) band shifts to 1592 cm^{-1}, and a newly formed ν(C=N) band appears at 1506 cm^{-1}. The ν(N–N) vibration is observed at 1111 cm^{-1}. The ν(C=S)/ν(C–S) bands appear at 1322 and 854 cm^{-1}. No ν(O–H), δ(C=S)/δ(C–S), or ν(C–O) bands were reported. The electronic spectrum of the free thiosemicarbazone ligand (Hbzpyetsc) shows an absorption band at 30,840 cm^{-1}, which can be attributed to $n \rightarrow \pi^*$ and $\pi \rightarrow \pi^*$ transitions within the conjugated ligand system. Upon complexation with Cd(II), this band shifts to 33,131 cm^{-1}, indicating changes in the electronic distribution as a result of coordination. Furthermore, a band observed at 23,600 cm^{-1} in the ligand spectrum shifts to 24,636 cm^{-1} in the complex and can be assigned to a metal-to-ligand charge transfer (MLCT) transition. These spectral changes confirm the interaction between the ligand and the Cd(II) center and support the formation of the coordination complex.

3.3. Hirshfeld surface analysis

Hirshfeld surface analysis gives detailed information on the interactions in the crystal structure. Crystal Explorer 3.1 software was used for this study [30]. Hirshfeld surface analysis was carried out to evaluate the nature and extent of intermolecular interactions with the percentage of the individual interactions of title complex. Figure 5 shows the various contacts on the Hirshfeld. The d_{norm} (normalized measure of intermolecular contact distances relative to van der Waals radii) (a), d_e (distance from the Hirshfeld surface to the nearest external atom) (b), shape index (property that reveals complementary surface shapes) (c), curvedness (measure of how much flat or curved the region is) (d), and fragment patches (shows which nearby molecules touch different parts of the surface) (e) were mapped using standard indices.

The d_{norm} was calculated using Equation 1.

$$d_{norm} = \frac{d_i - r_i vdw}{r_i vdw} + \frac{d_e - r_e vdw}{r_e vdw} \quad (1)$$

In Equation 1, rvdw is the van der Waals radius of atoms, while d_e denotes the distance from the Hirshfeld surface to the nearest external nucleus, and d_i is the analogous distance to the closest internal nucleus. Contacts shorter than the sum of the van der Waals radii appear as bright red spots. The d_{norm} surface is visualized using a red-white-blue colour scale. Interactions longer than the van der Waals radii are shown in blue, while contacts close to the van der Waals separation correspond to the white regions [31-34]. The shape index curve is useful for identifying the π-π stacking and surface matching. The red and triangular patterns observed on the shape index surface indicate the presence of π-π stacking interactions between aromatic rings, while the complementary red and blue regions in the neighbouring molecules reflect the degree of surface matching within the crystal lattice [35,36]. Such interactions are commonly observed in similar coordination complexes. Consecutive red and blue triangular regions around aromatic rings have also been reported in the literature [37], confirming that π-π stacking interactions are a characteristic feature in these types of systems. Curvedness measures how flat or curved the surface is at each point, and fragment path shows which parts of the surrounding molecule interact with different regions of the surface.

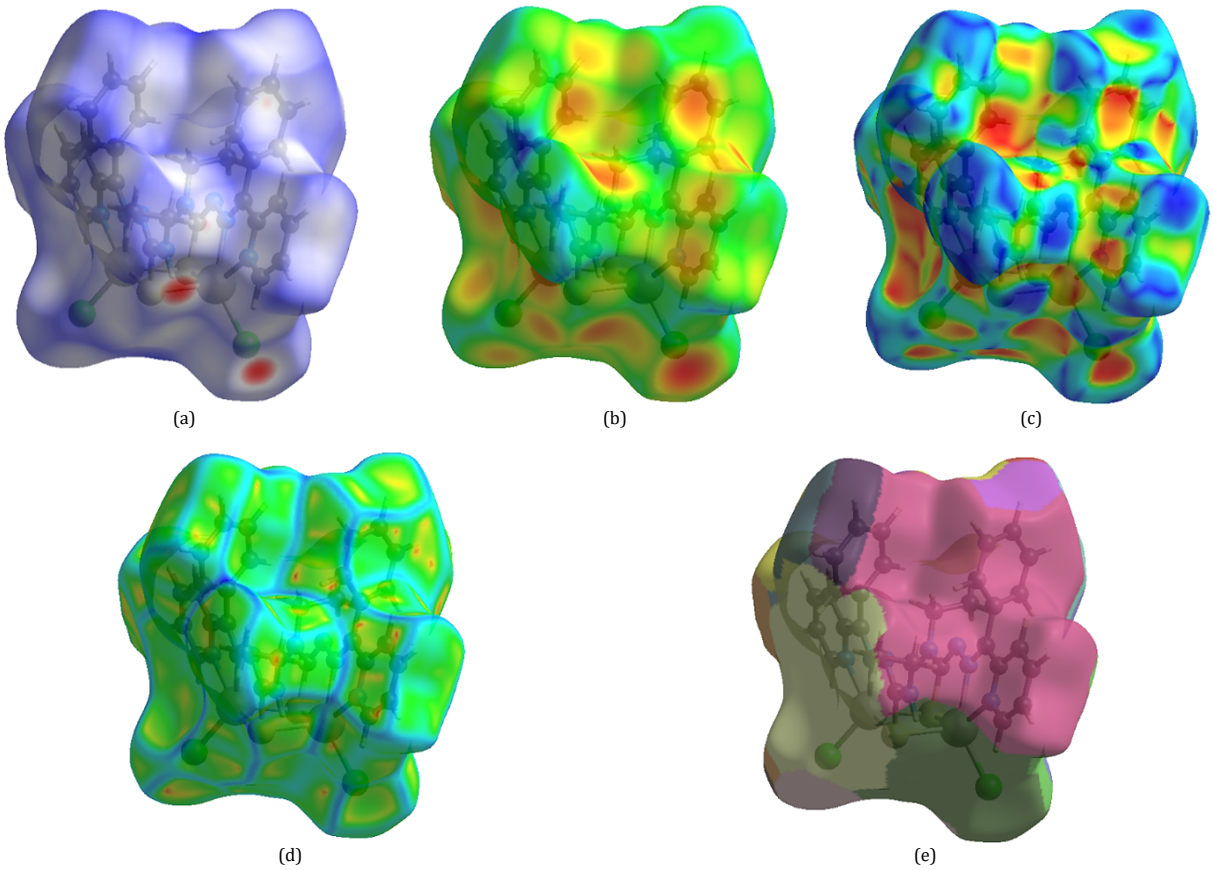

Figure 5. Hirshfeld surfaces mapped for (a) d_{norm} surfaces, (b) d_e, (c)shape index, (d) curvedness, and (e) fragment patch of $[Cd_2(bzpyetsc)_2(Cl)_2]$.

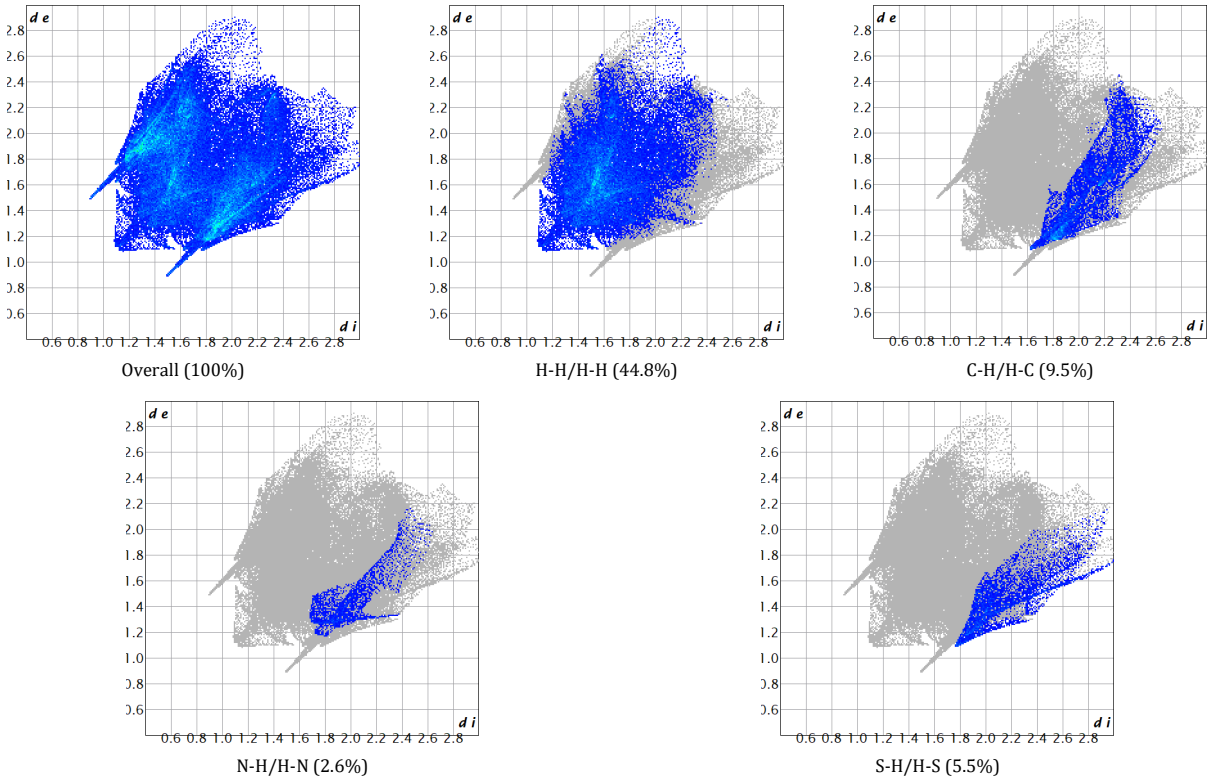

Figure 6. Relative individual contributions of the atoms in the title complex.

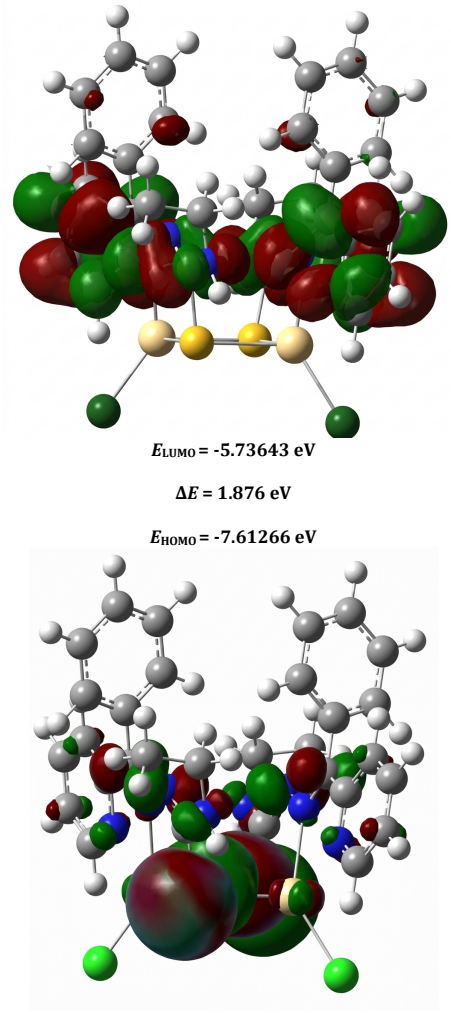

Figure 7. HOMO-LUMO plot of $[Cd_2(bzpyetsc)_2(Cl)_2]$.

In Figure 5, the blue lines on the curved surface indicate the edges and corners that are less involved in face-to-face contacts. In the fragmentation path light violet, green, and blue colours are observed. These colors themselves do not mean stronger or weaker interactions. They are just identifiers to see which parts of the molecule interact with which neighbors. Different colors indicate different region touching the neighboring molecule. The 2-dimensional fingerprint plot showing the main specific contribution of the atoms to the total surface is shown in Figure 6.

The most dominant interaction here is the H-H contact with 44.8%. The second most dominant interaction is C-H (9.5%). All other interactions are relatively small. While H···H interactions (30.3%) were reported as the second most dominant contacts in related Cd(II) complexes [38], in the present structure, they constitute the largest contribution to the Hirshfeld surface. This suggests that dispersive van der Waals interactions play a more prominent role in governing the crystal packing of the current complex.

3.4. HOMO-LUMO analysis

HOMO-LUMO analysis reveals that the HOMO is mainly located on the Cd metal, nitrogen atoms, and sulfur atoms. LUMO is in the nitrogen atom connected to the metal and the nearby regions. The HOMO-LUMO plot of the title complex is shown in Figure 7. The energy gap is found to be 1.876 eV. From the HOMO-LUMO values, all other important parameters of the complex can be calculated from the Koopmans theorem [39]. The ionization energy of the title complex (7.613 eV) indicates moderate to strong resistance to electron loss. According to Koopmans' theorem, the global reactivity parameters of the title complex are [40]: electron affinity (A) = 5.736 eV, chemical potential (μ) = -6.675 eV, global hardness (η) = 0.938 eV, global softness (S) = 1.066 eV^{-1} and electrophilicity index (ω) = 23.75 eV. These findings imply that the title complex has strong electronic stability and mild chemical reactivity. The comparatively high ionization potential (7.613 eV) indicates considerable resistance to electron removal, which means that the complex is difficult to oxidize. The significant electron affinity (5.736 eV) and high electrophilicity index (23.75 eV) indicate a strong inclination to take electrons, indicating a pronounced electrophilic nature. The system's negative chemical potential (-6.675 eV) indicates thermodynamic stability, whereas the moderate global hardness (0.938 eV) and the softness (1.066 eV^{-1}) show a balanced ability to resist and tolerate charge transfer. A band gap of 1.87 eV enables efficient absorption in the visible region, suggesting that the Cd(II) complex may be a potential candidate for visible light-driven photocatalytic applications such as organic dye degradation, environmental remediation, and hydrogen evolution [41].

3.5. Molecular electrostatic potential analysis

The MEP study was conducted to find the electronic distribution in the complex. It represents the electrostatic

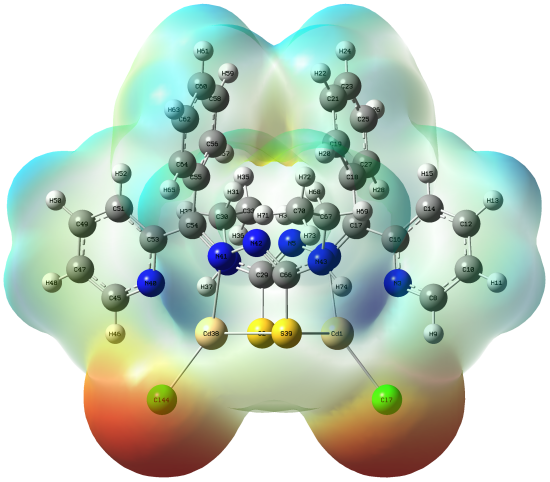

Figure 8. Electrostatic potential map of the title complex.

potential created by the nuclei and electrons of a molecule in a three-dimensional space, mapped onto an electron density surface. The MEP provides direct information on regions susceptible to electrophilic and nucleophilic attack [42]. The electrostatic potential map of the title complex is shown in Figure 8. As evident in Figure 8, the electron density is predominantly localized around the chlorine atoms. The red regions observed around Cl7 and Cl44 indicate areas of high electron density, while the green and blue areas correspond to the neutral and electron-deficient regions. The positively charged regions (blue) are associated with nucleophilic reactivity, whereas the negatively charged regions (red) are favorable for electrophilic attack. The localization of negative electrostatic potential around the electronegative atoms is consistent with previously reported MEP studies of coordination complexes, where halide and heteroatoms (such as N and S) typically exhibit regions of high electron density. Similar charge distribution patterns have been observed in related metal-ligand systems, supporting the reliability of the present electronic structure analysis [43-45].

4. Conclusions

In this research study, a Cd(II) complex with two NNS thiosemicarbazone-based donor ligands was synthesized and reported. The Cd(II) ion gives a distorted square pyramidal structure. The reported compound is a sulfur-bridged box dimer cadmium complex, which is rare for thiosemicarbazone ligands. The molecular structure of the complex is confirmed by the X-ray diffraction technique, elemental analysis, IR and UV spectroscopic methods. The title complex was further analyzed by density functional theorem. The compound was optimized and its bond lengths and bond angles were compared with the corresponding experimental values. The close agreement between the theoretical and experimental data demonstrates the reliability and accuracy of the computational study. HOMO-LUMO analysis indicated that the complex is electronically stable with moderate chemical reactivity. In addition, molecular electrostatic potential analysis was performed to determine the reactive hot spots. Hirshfeld surface analysis was performed to quantify the intermolecular interactions which are responsible for crystal packing and molecular stability.

Acknowledgements

The authors acknowledge Dr. Remalakshmi Poduval, Devasom Board College Thalayolaparamb, Kerala, for providing computational workspace.

Supporting information

CCDC-2523674 contains the supplementary crystallographic data for this paper. These data can be obtained free of charge via www.ccdc.cam.ac.uk/data_request/cif, or by e-mailing data_request@ccdc.cam.ac.uk, or by contacting The Cambridge Crystallographic Data Centre, 12 Union Road, Cambridge CB2 1EZ, UK; fax: +44(0)1223-336033.

Disclosure statement

Conflict of interest: The authors declare that we have no conflict of interest.
Ethical approval: All ethical guidelines have been adhered to in the work.
Sample availability: Samples of the compounds are available from the author and will be available on request.

CRediT authorship contribution statement

Conceptualization: Alan Mankottil Johnson, Nisha Kuttappan, Kannan Vellayan; Methodology: Alan Mankottil Johnson, Nisha Kuttappan ,Kannan Vellayan; Software: Alan Mankottil Johnson; Validation: Kannan Vellayan; Formal Analysis: Nisha Kuttappan, Kannan Vellayan; Investigation: Nisha Kuttappan, Resources: Alan Mankottil Johnson, Nisha Kuttappan, Kannan Vellayan; Data Curation: Alan Mankottil Johnson, Nisha Kuttappan, Kannan Vellayan; Writing - Original Draft: Alan Mankottil Johnson, Nisha Kuttappan, Kannan Vellayan; Writing - Review and Editing: Kannan Vellayan; Visualization: Alan Mankottil Johnson, Nisha Kuttappan; Supervision: Kannan Vellayan.

ORCID and Email

Alan Mankottil Johnson
alanjohnsonmankottil@gmail.com
https://orcid.org/0009-0003-2219-2082
Nisha Kuttappan
nichuanil@gmail.com
https://orcid.org/0009-0001-3579-1709
Kannan Vellayan
kannanpvl@gmail.com
https://orcid.org/0000-0003-2180-7834

References

[1]. Nozha, S. G.; Morgan, S. M.; Ahmed, S. E. A.; El-Mogazy, M. A.; Diab, M. A.; El-Sonbati, A. Z.; Abou-Dobara, M. I. Polymer complexes. LXXIV. Synthesis, characterization and antimicrobial activity studies of polymer complexes of some transition metals with bis-bidentate Schiff base. *J. Mol. Struct.* **2021**, *1227*, 129525.
[2]. Morgan, S.; El-Sonbati, A.; Eissa, H. Geometrical structures, thermal properties and spectroscopic studies of Schiff base complexes: Correlation between ionic radius of metal complexes and DNA binding. *J. Mol. Liquids* **2017**, *240*, 752–776.
[3]. Morrow, H. Cadmium and Cadmium Alloys. *Kirk-Othmer. Encyclopedia of Chemical Technology* **2010**, 1–36.

[4]. Abyar, S.; Khandar, A. A.; Salehi, R.; Abolfazl Hosseini-Yazdi, S.; Alizadeh, E.; Mahkam, M.; Jamalpoor, A.; White, J. M.; Shojaei, M.; Aizpurua-Olaizola, O.; Masereeuw, R.; Janssen, M. J. In vitro nephrotoxicity and anticancer potency of newly synthesized cadmium complexes. *Sci. Rep.* **2019**, *9* (1), 14686 https://doi.org/10.1038/s41598-019-51109-9.

[5]. Gupta, V. K.; Sharma, N.; Sharma, A.; Teraiya, S. B.; Parmar, N. J.; Sharma, D. Crystallographic and Hirshfeld surface analysis of 10-(4-chlorophenyldiazenyl)-3-(3-chlorophenyl)-1-methyl-3,5a,6,11b-tetrahydro-5H-benzopyrano[4',3'-4,5]pyrano[2,3-c]pyrazole. *Eur. J. Chem.* **2025**, *16* (3), 311–318.

[6]. Xu, J.; Wang, X.; Zhang, X.; Zhang, Y.; Yang, Z.; Li, S.; Tao, L.; Wang, Q.; Wang, T. Room-temperature self-healing supramolecular poly urethanes based on the synergistic strengthening of biomimetic hierarchical hydrogen-bonding interactions and coordination bonds. *Chemical Engineering Journal* **2023**, *451*, 138673.

[7]. Dong, W.; Akogun, S. F.; Zhang, Y.; Sun, Y.; Dong, X. A reversible "turn-on" fluorescent sensor for selective detection of Zn2+. *Sensors and Actuators B: Chemical* **2017**, *238*, 723–734.

[8]. Kumaravel, G.; Ponya Utthra, P.; Raman, N. Exploiting the biological efficacy of benzimidazole based Schiff base complexes with l-Histidine as a co-ligand: Combined molecular docking, DNA interaction, antimicrobial and cytotoxic studies. *Bioorg. Chem.* **2018**, *77*, 269–279.

[9]. Mautner, F. A.; Fischer, R. C.; Reichmann, K.; Gullett, E.; Ashkar, K.; Massoud, S. S. Synthesis and characterization of 1D and 2D cadmium(II)-2,2′-bipyridine-N,N′-dioxide coordination polymers bridged by pseudohalides. *J. Mol. Struc.* **2019**, *1175*, 797–803.

[10]. Banu, K. S.; Mondal, S.; Guha, A.; Das, S.; Chattopadhyay, T.; Suresh, E.; Zangrando, E.; Das, D. Synthesis, characterization and luminescence properties of polymeric cadmium(II) complexes with imidazole and its derivatives mediated by thiocyanate and dicyanamide anions. *Polyhedron* **2011**, *30* (1), 163–168.

[11]. Banerjee, A.; Maiti, P.; Chattopadhyay, T.; Banu, K. S.; Ghosh, M.; Suresh, E.; Zangrando, E.; Das, D. Syntheses and crystal structures of cadmium(II)X2-hexamethylenetetramine (X=Br−/I−/SCN−) coordination polymers having different dimensionality. *Polyhedron* **2010**, *29* (3), 951–958.

[12]. Saren, D.; Bodensteiner, M.; Manna, S. C. Dinuclear cadmium(II) complexes with distorted octahedral/monocapped trigonal prism coordination geometries: synthesis, crystal structure, DFT/TD-DFT calculation and photocatalytic degradation of methylene blue. *Polyhedron* **2024**, *254*, 116936.

[13]. Du, M.; Zhao, X. Synthesis, characterization and crystal structures of new MnII, FeII and AgI complexes with an angular dipyridyl ligand 2,5-bis(4-pyridyl)-1,3,4-oxadiazole. *J. Mol. Struc.* **2004**, *694* (1-3), 235–240.

[14]. Rhoufal, F.; Bentiss, F.; Guesmi, S.; Ketatni, E. M.; Saadi, M.; El Ammari, L. Crystal structure, spectroscopic characterization and Hirshfeld surface analysis of *trans*-diaqua[2,5-bis(pyridin-4-yl)-1,3,4-oxadiazole]dithiocyanatonickel(II). *Acta Crystallogr. E Cryst. Commun.* **2019**, *75* (7), 1046–1050.

[15]. Arshad, T.; Khan, K. M.; Rasool, N.; Salar, U.; Hussain, S.; Asghar, H.; Ashraf, M.; Wadood, A.; Riaz, M.; Perveen, S.; Taha, M.; Ismail, N. H. 5-Bromo-2-aryl benzimidazole derivatives as non-cytotoxic potential dual inhibitors of α -glucosidase and urease enzymes. *Bioorg. Chem.* **2017**, *72*, 21–31.

[16]. Nisha, K. Transition Metal Complexes of ONS and NNS Donor Thiosemicarbazones: Crystal Structures and Spectral Studies. Ph.D. Thesis, Cochin University of Science and Technology (CUSAT), Kochi, India, 2016.

[17]. Bruker (2008). SMART, SAINT. Bruker AXS Inc., Madison, Wisconsin, USA.

[18]. Sheldrick, G. M. (1996). SADABS. University of Göttingen, Germany.

[19]. Sheldrick, G. M. A short history of*SHELX*. *Acta Crystallogr. A. Found Crystallogr.* **2007**, *64* (1), 112–122.

[20]. Sheldrick, G. M. SHELXS-97 and SHELXL-97 Program for Crystal Structure Solution and Refinement. University of Gottingen, Germany, Germany, 1997.

[21]. Brandenburg, K. (1999). DIAMOND. Crystal Impact GbR, Bonn, Germany.

[22]. Frisch, M. J.; Trucks, G. W.; Schlegel, H. B.; Scuseria, G. E.; Robb, M. A.; Cheeseman, J. R.; Montgomery, J. A.; Vreven, T.; Kudin, K. N.; Burant, J. C.; Millam, J. M.; Iyengar, S. S.; Tomasi, J.; Barone, V.; Mennucci, B.; Cossi, M.; Scalmani, G.; Rega, N.; Petersson, G. A.; Nakatsuji, H.; Hada, M.; Ehara, M.; Toyota, K.; Fukuda, R.; Hasegawa, J.; Ishida, M.; Nakajima, T.; Honda, Y.; Kitao, O.; Nakai, H.; Klene, M.; Li, X.; Knox, J. E.; Hratchian, H. P.; Cross, J. B.; Adamo, C.; Jaramillo, J.; Gomperts, R.; Stratmann, R. E.; Yazyev, O.; Austin, A. J.; Cammi, R.; Pomelli, C.; Ochterski, J. W.; Ayala, P. Y.; Morokuma, K.; Voth, G. A.; Salvador, P.; Dannenberg, J. J.; Zakrzewski, V. G.; Dapprich, S.; Daniels, A. D.; Strain, M. C.; Farkas, O.; Malick, D. K.; Rabuck, A. D.; Raghavachari, K; Foresman, J. B.; Ortiz, J. V.; Cui, Q.; Baboul, A. G.; Clifford, S.; Cioslowski, J.; Stefanov, B. B.; Liu, G.; Liashenko, A.; Piskorz, P.; Komaromi, I.; Martin, R. L.; Fox, D. J.; Keith, T.; Al-Laham, M. A.; Peng, C. Y.; Nanayakkara, A.; Challacombe, M.; Gill, P. M. W.; Johnson, B.; Chen, W.; Wong, M. W.; Gonzalez, C.; Pople, J. A. Gaussian, Inc., Wallingford CT, 2004.

[23]. Yang, Y.; Weaver, M. N.; Merz, K. M. Assessment of the "6-31+G** + LANL2DZ" Mixed Basis Set Coupled with Density Functional Theory Methods and the Effective Core Potential: Prediction of Heats of Formation and Ionization Potentials for First-Row-Transition-Metal Complexes. *J. Phys. Chem. A.* **2009**, *113* (36), 9843–9851.

[24]. Padmaja, L.; Ravikumar, C.; Sajan, D.; Hubert Joe, I.; Jayakumar, V. S.; Pettit, G. R.; Faurskov Nielsen, O. Density functional study on the structural conformations and intramolecular charge transfer from the vibrational spectra of the anticancer drug combretastatin-A2. *J. Raman Spectroscopy* **2008**, *40* (4), 419–428.

[25]. Poiyamozhi, A.; Sundaraganesan, N.; Karabacak, M.; Tanrıverdi, O.; Kurt, M. The spectroscopic (FTIR, FT-Raman, UV and NMR), first-order hyperpolarizability and HOMO–LUMO analysis of 4-amino-5-chloro-2-methoxybenzoic acid. *Journal. of. Molecular. Structure.* **2012**, *1024*, 1–12.

[26]. Suresh, C. H.; Remya, G. S.; Anjalikrishna, P. K. Molecular electrostatic potential analysis: A powerful tool to interpret and predict chemical reactivity. *WIREs. Comput. Mol. Sci.* **2022**, *12* (5), e1601 https://doi.org/10.1002/wcms.1601.

[27]. Fuentealba, P.; Florez, E.; Tiznado, W. Topological Analysis of the Fukui Function. *J. Chem. Theory. Comput.* **2010**, *6* (5), 1470–1478.

[28]. López-Torres, E.; Mendiola, M. A.; Pastor, C. J.; Pérez, B. S. Versatile Chelating Behavior of Benzil Bis(thiosemicarbazone) in Zinc, Cadmium, and Nickel Complexes. *Inorg. Chem.* **2004**, *43* (17), 5222–5230.

[29]. Yadav, P. N.; Mahiya, K.; Tharu, K. B.; Punniyamoorthy, S.; Shrestha, A.; Bhattarai, N. P.; Pokharel, Y. R. N(3)-substituted thiophene-2-carboxaldehyde thiosemicarbazones compounds and their copper(II) complexes: Synthesis, characterization, in silico study and anticancer activity. *Polyhedron* **2026**, *289*, 118022.

[30]. Spackman, P. R.; Turner, M. J.; McKinnon, J. J.; Wolff, S. K.; Grimwood, D. J.; Jayatilaka, D.; Spackman, M. A. *CrystalExplorer*: a program for Hirshfeld surface analysis, visualization and quantitative analysis of molecular crystals. *J. Appl. Crystallogr.* **2021**, *54* (3), 1006–1011.

[31]. Al-Wahaibi, L. H.; Joubert, J.; Blacque, O.; Al-Shaalan, N. H.; El-Emam, A. A. Crystal structure, Hirshfeld surface analysis and DFT studies of 5-(adamantan-1-yl)-3-[(4-chlorobenzyl)sulfanyl]-4-methyl-4H-1,2,4-triazole, a potential 11β-HSD1 inhibitor. *Sci. Rep.* **2019**, *9* (1), 19745 https://doi.org/10.1038/s41598-019-56331-z.

[32]. Spackman, M. A.; Jayatilaka, D. Hirshfeld surface analysis. *CrystEngComm* **2009**, *11* (1), 19–32.

[33]. Odame, F.; Madanhire, T.; Hosten, E. C. Crystal Structure and Hirshfeld Surface Analysis of 3-(pyrrolidine-1-carbonyl)-2H-Chromen-2-One. *J. Struct. Chem.* **2024**, *65* (7), 1305–1316.

[34]. Odame, F.; Madanhire, T.; Hosten, E. C.; Lobb, K. Crystal Structure, Hirshfeld Surface Analysis and Computational Studies of Two Benzo[b][1,4]Diazepine Derivatives. *J. Struct. Chem.* **2023**, *64* (12), 2326–2342.

[35]. Tsering, D.; Dey, P.; Kapoor, K. K.; Seth, S. K. An Energetic and Topological Approach to Understanding the Interplay of Noncovalent Interactions in a Series of Crystalline Spiropyrrolizine Compounds. *ACS. Omega* **2024**, 36242–36258 https://doi.org/10.1021/acsomega.4c02511.

[36]. Gumus, I.; Solmaz, U.; Binzet, G.; Keskin, E.; Arslan, B.; Arslan, H. Hirshfeld surface analyses and crystal structures of supramolecular self-assembly thiourea derivatives directed by non-covalent interactions. *J. Mol. Struc.* **2018**, *1157*, 78–88.

[37]. Al-Jibori, S. A.; Al-Jibori, G. H.; Ashfaq, M.; Khalil, T.; Laguna, M.; Wagner, C.; Tahir, M. N.; Al-Janabi, A. S. Synthesis, characterization, crystal structure, Hirshfeld surface analysis of Cd(II)-1, 2-benzisothiazol-3(2H)-one complexes. *J. Mol. Struc.* **2023**, *1289*, 135803.

[38]. Akbari, Z.; Montazerozohori, M.; Hoseini, S. J.; Naghiha, R.; Hayati, P.; Bruno, G.; Santoro, A.; White, J. M. Synthesis, crystal structure, Hirshfeld surface analyses, antimicrobial activity, and thermal behavior of some novel nanostructure hexa-coordinated Cd(II) complexes: Precursors for CdO nanostructure. *Applied. Organom. Chem.* **2021**, *35* (5), e6181 https://doi.org/10.1002/aoc.6181.

[39]. Koopmans, T. Über die Zuordnung von Wellenfunktionen und Eigenwerten zu den Einzelnen Elektronen Eines Atoms. *Physica* **1934**, *1*, 104–113.

[40]. Johnson, A. M.; V, K.; K., N. A theoretical studies on the energetic properties of triazole-benzene and triazole-pyridine derivatives. *J. Mol. Model.* **2025**, *31* (9), 261 https://doi.org/10.1007/s00894-025-06484-8.

[41]. Qi, L.; Yu, J.; Jaroniec, M. Preparation and enhanced visible-light photocatalytic H2-production activity of CdS-sensitized Pt/TiO2 nanosheets with exposed (001) facets. *Phys. Chem. Chem. Phys.* **2011**, *13* (19), 8915.

[42]. Politzer, P.; Laurence, P. R.; Jayasuriya, K. Molecular electrostatic potentials: an effective tool for the elucidation of biochemical phenomena. *Environ. Health Perspect.* **1985**, *61*, 191–202.

[43]. El-Gammal, O.; Rakha, T.; Metwally, H.; Abu El-Reash, G. Synthesis, characterization, DFT and biological studies of isatinpicolino hydrazone and its Zn(II), Cd(II) and Hg(II) complexes. *Spectrochimica Acta Part A: Molecular and Biomolecular Spectroscopy* **2014**, *127*, 144–156.
[44]. Mchiri, C.; Nasri, H.; Frochot, C.; Acherar, S. Distorted five-coordinate square pyramidal geometry of a cadmium(II) complex containing a 2-methylimidazole ligand: Crystal structure and axial ligand effect on spectroscopic properties. *Polyhedron* **2019**, *173*, 114107.
[45]. Bencini, A.; Bianchi, A.; Del Piero, S.; Giorgi, C.; Melchior, A.; Portanova, R.; Tolazzi, M.; Valtancoli, B. Coordination Features of a Polyaza-Bipyridine-Macrocyclic Ligand toward Co(II) and Cd(II) in Water and Dimethylsulfoxide. *J. Solution. Chem.* **2008**, *37* (4), 503–517.